Surface features of TiO2 nanoparticles: combination modes of adsorbed CO probe the stepping of (101) facets

UNIVERSITÀ DEGLI STUDI DI TORINO

Surface features of TiO_2 nanoparticles: combination modes of adsorbed CO probe the stepping of (101) facets

Chiara Deiana,[a] Gloria Tabacchi,[b] Valter Maurino,[a] Salvatore Coluccia,[a] Gianmario Martra[a] and Ettore Fois[b*]

Integrated studies of CO adsorption on TiO_2 materials of different morphology and surface complexity identify, for the first time, frustrated translational CO modes by detecting their combination with the CO stretching mode (νCO). All the considered materials exhibit IR spectra with low-intensity bands in the 2235-2205 cm^{-1} range, a region where components due to strong Lewis acid Ti^{4+} sites may be present as well. These observations lead to a powerful method for associating high-wavenumber bands to TiO_2 surface features and interpreting IR spectra of drastically complex/defective TiO_2 materials. The proposed band assignment is based on vibrational analyses of CO/TiO_2 theoretical models, indicating that the frustrated translational mode with frequency in the 30-50 cm^{-1} range involved in the observed combination bands is perpendicular to the Ti^{4+} rows. Our results reveal that this low-energy CO mode is much more sensitive than νCO in probing the TiO_2 surface topography, and that its higher-energy components can be specifically associated to the presence of steps on the (101) faces. In a broader perspective, the frustrated translational CO mode surface sensitivity could become a key tool for detecting specific defective sites on TiO_2 surfaces.

Introduction

Understanding how reactivity is related to structure is a crucial issue for nanostructured titania, a key material for sustainable nanotechnologies, from energy production[1-3] to pollutants abatement.[4, 5]
Among TiO_2 polymorphs, anatase is widely employed because of its higher activity[6, 7] and, consequently, a number of preparation methods of TiO_2 anatase nanoparticles (NP) have been developed, ranging from commercially exploited sol-gel and pyrolysis (as for the well-known TiO_2 P25 by Evonik) procedures, to hydrothermal synthesis in the presence of shape-controllers.[8, 9] In many cases, the most frequently observed surfaces for such TiO_2 NP are of the (101) type, because of its thermodynamic stability.[10, 11]
However, stepping of (101) surfaces can occur, resulting in local structures with a different reactivity.[12] Moreover, peculiar surface terminations can be present in NP at edges and corners among different facets, as in the case of the so-called α sites, characterized by a higher Lewis acidity with respect to sites exposed at the (101) faces, and suggested to be responsible for important aspects of the surface reactivity.[12, 13] In spite of the number of related studies, the geometric structure and chemical environment of these reactive sites is not known yet.
Such a lack of information is motivating increasing research efforts aimed at elucidating the structure of the exposed Ti^{4+} sites, but the very complex nature of titania nanopowders prevents the use of standard single-crystal characterization techniques and represents a major obstacle to this goal.
Among the number of available surface techniques, spectroscopic methods are particularly suited for exploring structure and reactivity of surface sites. Since the pioneristic work of Eischens et al,[14] IR spectroscopy of adsorbed carbon monoxide is one of the most widely employed experimental methods for the investigation, at a molecular level, of the physical-chemical surface features of solids. Indeed, a broad variety of materials, ranging from single crystals[15] to finely divided solids including

nanomaterials, even of the micro- and mesoporous types,[16] may be characterized by using CO as a probe molecule, which can adsorb on zerovalent and cationic metal sites and presents one single internal C-O vibrational mode (νCO). The main source of information is the perturbation of this internal stretching mode, that primarily depends on the nature and strength of the interaction with the adsorbing sites. Moreover, the effects of adsorbate-adsorbate interactions on the shape and position of the νCO absorption band, generally investigated by using $^{12}CO/^{13}CO$ mixtures,[17] may provide further insight about the arrangements of surface sites.[18] It should however be pointed out that also the investigation of low-energy CO external modes could be of outmost relevance in this context. Indeed, the adsorption of CO on a surface should result in five low-frequency vibrational modes for the surface-CO bond: one absorbing site-C stretching, doubly degenerate frustrated rotational modes (librational modes) and doubly degenerate frustrated translational modes (tangential motions of CO along the surface). Understanding of phenomena like desorption of adsorbed molecules, the coupling of their vibrations to the substrate heat bath[19] and diffusion processes would greatly benefit from the knowledge of these modes. For instance, the frequency of frustrated translations can help in determining the steepness of the potential energy surface wells.[20] Moreover, frustrated translations have been proposed to respond to the presence of step sites on halides and oxides,[21] as well as librational modes were reported to be more sensitive than the internal CO stretching to the structure of carbonylic complexes in zeolites.[22]

Direct evidence for some of the external modes can be obtained on single crystals by electron energy loss spectroscopy (EELS)[23] or helium-atom scattering (HAS) both on metals[24] and oxides.[25] In principle, such information may also be deduced by IR, provided the availability of sources bright enough in the Far-IR region, as synchrotron radiation is.[26] Since conventional black-body sources are strong enough relative to thermal fluctuation of the systems only in the spectral region above ca. 400 cm^{-1}, the metal-carbon stretch vibration for CO on metals could be observed by infrared-reflection absorption spectroscopy (IRRAS).[27] However, IR absorption due to frustrated rotations and translations is not actually accessible through this technique because they occur at lower frequency, as well as the surface-carbon stretch for CO adsorbed on oxides or halides. Information on these modes are then extracted from their combination with the internal stretching mode of adsorbed CO. By adopting such an approach, important data on cation-carbon stretching of CO adsorbed on microcrystalline oxides[28, 29] or zeolites,[30] frustrated rotation of CO on microcrystalline MgO[29] and on NaCl films[31] were gathered.

A similar strategy was followed in this work for determining the external modes of CO adsorbed on TiO_2 nanoparticles through experimental methods and calculations. Such kind of integrated. approaches may provide relevant insight on TiO_2 structure-reactivity correlations.[13, 32]

With the aim of capturing the spectroscopic fingerprint of these elusive modes, three materials have been considered: (i) commercial TiO_2 P25, a landmark in the field of photocatalytic applications,[33] which is characterized by a very complex morphology exposing α sites as well; (ii) TiO_2 HT,[13] a nanomaterial with a well-defined morphology that does not expose α sites, which, in terms of complexity, could be considered to be in between TiO_2 P25 and ideal systems such as single crystals; (iii) TiO_2 HT after etching with HF.

Experimental

Materials

The samples considered were: i) TiO_2 Evonik P25, formerly Degussa (ca. 80% anatase, 20% rutile) with SSA_{BET} of ca. 55 $m^2 \cdot g^{-1}$ for the pristine material, that decreases to 40 $m^2 \cdot g^{-1}$ after outgassing at 873 K; ii) TiO_2 HT (100% anatase), prepared by hydrothermal conditions, and characterized by initial SSA_{BET} of ca. 42 $m^2 \cdot g^{-1}$, that decreases to ca. 37 $m^2 \cdot g^{-1}$ after outgassing at 873 K. Further details on the

preparation and characterization of the two materials are reported in our previous work.[13] iii) The etching of TiO_2 HT was performed following the work of Taguchi et al.,[34] by suspending the nanoparticles in HF 10% (w/w) in a sealed Teflon container. The suspension was maintained at 313 K under magnetic stirring for 2 hours. The etched nanoparticles were centrifuged and washed with water then treated at 673 K in air for 2 hours in order to remove surface adsorbed fluorides. The obtained material will be hereafter referred to as TiO_2 HT-HF.
For the samples treatment and IR measurements, high purity O_2 and CO (99.999%, Praxair) were used, after liquid nitrogen trapping.

Methods
IR MEASUREMENTS. The samples were pressed in self-supporting pellets and placed in quartz cells with KBr windows, designed to carry out spectroscopic measurements at ca. 100 K (by cooling with liquid nitrogen), and connected to conventional vacuum lines (residual pressure $\leq 1 \times 10^{-5}$ mbar), allowing the thermal treatment and adsorption-desorption experiments to be carried out *in situ*. The "optical thickness" of the pellets was of ca. 10-15 $m^2 \cdot g^{-1}$.
The samples were pretreated before IR measurements at 873 K for 60 min, and then contacted with O_2 (6 mbar) at the same temperature for 60 min. The samples were cooled to 473 K in the presence of oxygen and then further cooled down to room temperature. For specific measurements, the sample was rehydrated by contact with 20 mbar of H_2O vapour, and the treatment was repeated, but limiting at 573 K the temperature of the initial outgassing. At the end of the procedure, all the samples, white in colour, were expected to be fully oxidized and to expose only Ti^{4+} ions as surface Lewis acid centres.[35] For this reason, only defect-free surfaces were considered for modelling.
The measurements were carried out with a Bruker IFS28 spectrometer equipped with an MCT detector. The spectra, collected at resolution 2 cm^{-1}, are reported in Absorbance, after subtraction of spectra obtained before CO admission as a background.
HIGH RESOLUTION TRANSMISSION ELECTRON MICROSCOPY (HR-TEM) images of the nanoparticles (powder grains "dry" dispersed on lacey carbon Cu grids) were collected using a JEOL 3010-UHR microscope operated at an acceleration potential V=300 kV.
THEORETICAL MODELING OF CO ADSORPTION. Carbon monoxide adsorption on TiO_2 was simulated in the $\theta \rightarrow 1$ limit by using periodic slab models of anatase (101) facets, which expose pentacoordinated Ti sites and are predominant in both TiO_2 HT and TiO_2 P25 nanoparticles.[13] Also (110) facets, which expose tetracoordinated Ti sites, were considered. Regular facets were modelled. The PBE approximation[36] to Density Functional Theory for the electronic structure calculations was employed. Electronic states were expanded in planewaves up to a cutoff of 80 Ry (320 Ry for the electronic density) and norm conserving pseudopotentials[37] were adopted. In the case of Ti, a full core pseudopotential (i.e. a Ti^{4+} is considered) was adopted along with the Non Linear Core Correction scheme.[38] By this pseudopotential choice, structural, vibrational and electronic properties of a variety of Ti-containing systems were properly reproduced.[39-44] Geometry optimizations were performed at fixed volume in the slab approximation.[44-46] In all the slab calculations, the Γ point only was considered; tests of the convergence with respect of planewave cutoff and Brillouin Zone sampling are reported in our previous work.[13] The (101) slab consists of 6 Ti_6O_{12} layers (stoichiometry: $Ti_{36}O_{72}$), with area of 11.355×9.514 $Å^2$; and contains 6 CO molecules. The (110) slab consists of 8 Ti_4O_8 layers (stoichiometry: $Ti_{32}O_{64}$), with area of 10.7056×9.514 $Å^2$, and bears 4 CO molecules. In both cases, a vacuum region of 12 Å, perpendicular to the slab surface, was considered in order to minimize the interactions between periodically repeated slabs. The area was determined from the experimental lattice parameters of anatase.[47] A maximum force of 5×10^{-5} Hartree/Bohr was chosen as convergence criterion in the optimizations. The atoms of the bottom TiO_2 layer were kept fixed in their crystallographic positions during optimizations. Calculated relative slab stabilities, which are in line

with literature data,[10, 11] are reported in Table S1 in the Electronic Supplementary Information, hereafter ESI.
Such a computational scheme has been shown to provide a proper description of CO adsorption on various types of TiO_2 anatase facets.[13] Besides perfectly ordered models (i.e., at 0 K), systems characterized by thermal disorder were considered as well. Thermally disordered models were obtained by starting from the symmetric optimized structures and performing Car Parrinello molecular dynamics simulations for 1 ps at 100 K.[48] From such trajectories, the final "thermally disordered" configurations were optimized. The energy difference between the thermally disordered optimized structures and the corresponding ordered ones amounted to only 1 kcal mol^{-1}, indicating that disordered structures are thermally accessible in the 60-100 K range and should therefore be considered in band assignment, as clearly shown in Ref [13]. The same slab models were used for the calculation of adsorbed CO in the $\theta \rightarrow 0$ limit for both (101) and (110) surfaces, by considering only one CO molecule per slab (actually corresponding to $\theta=1/6$ and $\theta=1/4$ for the (101) and (110) slab, respectively). Geometries were optimized by adopting the above described protocol for ordered $\theta=1$ systems. Harmonic frequencies were obtained numerically by performing finite difference calculations on the optimized structures. As for the geometry optimization runs, the bottom layer atom positions have been kept fixed in the frequency calculations. All discussed structures are characterized by positive frequencies.
Calculations have been performed with the CPMD code.[49] From the calculated vibrational eigenvectors, modes localization was estimated by calculating the Participation Ratio.[50]

Results and discussion

Experimental IR data

Figure 1A shows the spectra of CO adsorbed at ca. 100 K on TiO_2 P25 at progressively decreasing coverage, from the presence of 45 mbar CO to outgassing for 10 minutes. The analysis of the overall pattern and the unambiguous assignment of the main component has been the subject of a previous study,[13] also in comparison with literature data on CO on (101) TiO_2 anatase single crystal,[51] and a summary of the assignment of the various components is listed in Table S2 in the ESI.
Here, this collection of data is reported in order to highlight two features:
i) the main peak at 2179 cm^{-1}, due to CO adsorbed on (101) TiO_2 anatase surfaces, appeared less reversible than components at lower frequency, and, for CO pressure < 0.1 mbar the spectral profiles appeared essentially constituted only by this signal and the shoulder at 2183 cm^{-1}, related to CO on (110) TiO_2 anatase facets (black curves). It must be noticed that in this condition the intensity of the main peak was only slightly lower than in the presence of 45 mbar CO (panel A, top grey curve), when all Ti^{4+} sites were occupied by probe molecules.[13] Thus, the CO coverage attained after depletion of all the νCO components at frequency lower than 2170 cm^{-1} will be hereafter referred as $\theta_{CO}(101) \rightarrow 1$.
ii) at frequency > 2200 cm^{-1}, a proper zoom (displayed in the inset) revealed the presence of a very weak component initially located at 2212 cm^{-1}, and of a slightly more intense band initially located at 2206 cm^{-1}, assigned to CO on the so called "α" sites, i.e. four-coordinated Ti^{4+} cations, traditionally proposed to be exposed on high index crystal planes, as well as on some edges.[35] By decreasing the CO coverage, both signals exhibited an up-shift, accompanied by a quite complex evolution in the case of the high frequency component (*vide infra*). Noticeably, this component was depleted *before* the band due to CO on α sites (thicker curve). Such difference in reversibility indicated *that the signal initially located at 2212 cm^{-1} cannot be due to CO molecules probing Ti^{4+} sites with higher Lewis acidity than α sites*. If not, conversely, they should adsorb CO in a less reversible way, as expected for CO interacting with cationic sites in a d^0 electronic configuration.[16]

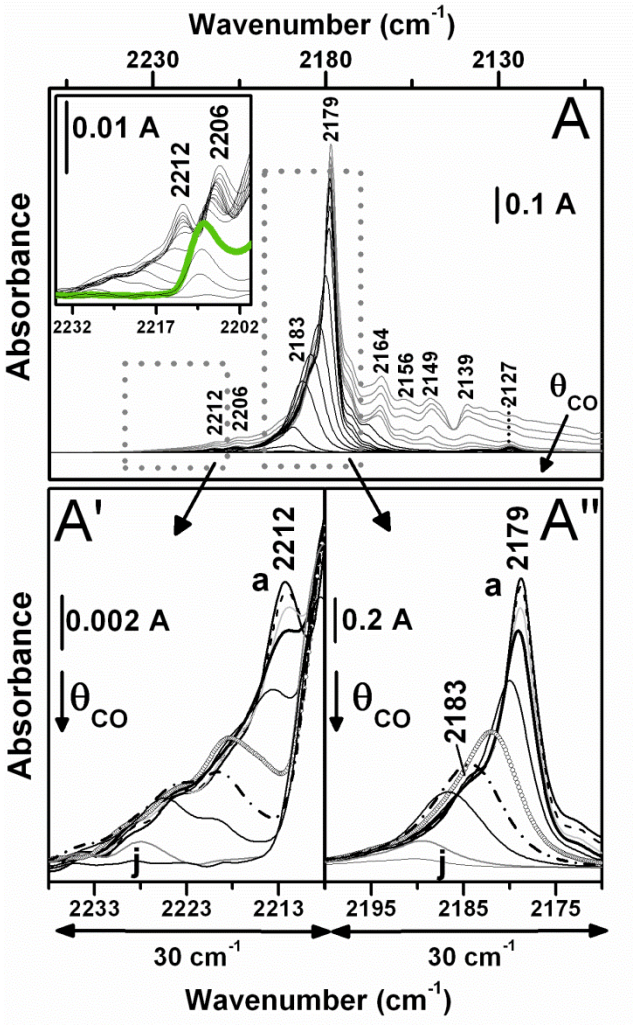

Fig.1 IR spectra of decreasing amount of CO adsorbed at ca. 100 K on TiO_2 P25 outgassed at 873 K. Panel A (2260-2100 cm^{-1}): spectra collected in conditions ranging from the presence of 45 to 0.6 mbar (grey curves) and from the presence of 0.1 mbar to outgassing for 10 minutes at ca. 100 K (black curves). Decreasing CO coverages are as in the sense of the arrow. Inset: zoomed view of the 2235-2200 cm^{-1} region. Panels A' and A": zoomed view, in the 2238-2008 cm^{-1} and 2200-2170 cm^{-1} range, respectively, of the black curves in panel A. Decreasing CO coverages are in the sense of lettering.

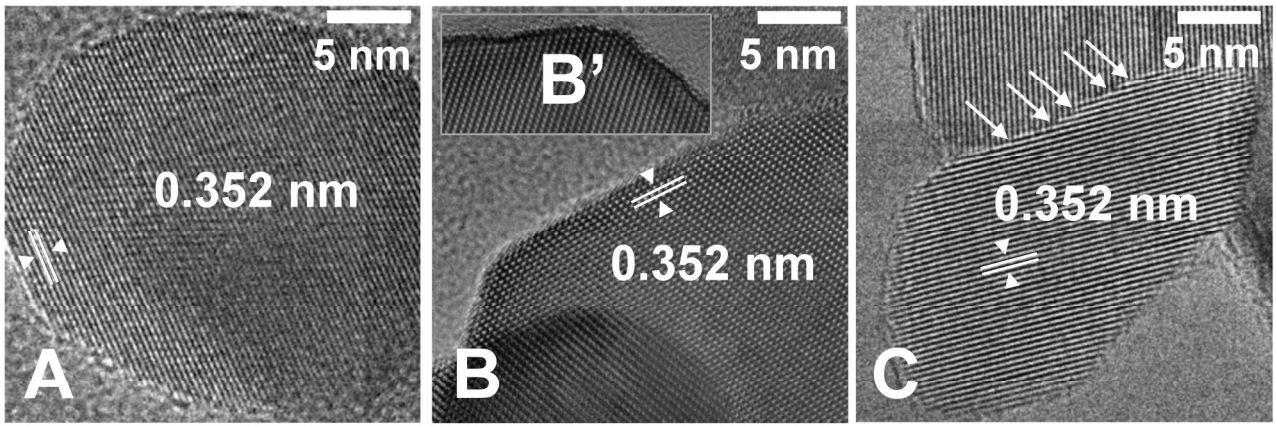

Fig.2 HRTEM images representative of the surface terminations of: A) TiO_2 P25 (original magnification 500k ×); B) TiO_2 HT (original magnification 800k ×); inset B': evidence of the presence of steps on a (101) facet (original magnification 1000k ×); C) TiO_2 HT-HF (original magnification 600k ×). At high magnification, lattice fringes due to phase contrast appeared, running parallel to one of the main borders (panel B').

An interesting insight was provided by the synoptic inspection of the 2238-2208 and 2200-2170 cm^{-1} ranges (Figure 1, panels A' and A'', respectively), which highlighted the parallel evolution of the two patterns (differing in intensity of ca. 2 orders of magnitude in favour of the lower frequency one), strongly suggesting they should be related to each other. In this respect, it must be noticed that at very low CO coverage any signal was no-longer present in the 2235-2208 cm^{-1} range (except the onset of the band due to CO on α sites), whereas a band was still observed at 2190 cm^{-1} (curves j, panels A,A'). However, such discrepancy can be reasonably ascribed to the huge difference in intensity, likely resulting in the vanishing below the detection limit of the weakest signals at high frequency. Moreover, the pattern in the 2238-2208 cm^{-1} range appeared more structured, and its subbands exhibited a complex evolution. For the sake of clarity, these features will be commented on in the following. The presence of the onset of the signal due to CO on α sites, partly overlapped to the band at 2212 cm^{-1}, and the coexistence of components due to CO on (101) and (110) surfaces in the profile at lower frequency rendered difficult a more detailed analysis. To this aim, two other types of TiO_2 samples were considered, one constituted by nanoparticles (NP) with a well-defined truncated bipyramidal shape (TiO_2 HT), with lateral faces corresponding to (101) surfaces,[13] and the second resulting from the etching of such nanoparticles with HF (TiO_2 HT-HF), following the approach adopted in a seminal work on the erosion of well-shaped MgO nanoparticles by treatment with H_2O vapour.[52] From a morphological point of view (see HRTEM images in Figure 2 and Figure S1 in the ESI), this corresponded to move from titania NP with rough borders as those of TiO_2 P25 (panel A), to TiO_2 HT with regular (101) terminations (parallel to lattice fringes 0.352 nm apart, corresponding to the $d_{(101)}$ spacing)[53] exhibiting few steps (panel B), and to the heavily stepped (101) surface profiles of TiO_2 HT-HF (panel C), directly derived from the previous material.

The whole series of spectra of TiO_2 HT in the presence of decreasing amount of adsorbed CO is reported in Figure S2 in the ESI. For the sake of comparison with Figure 1A', A", a selection of these data are displayed in Figure 3, starting from the spectrum collected after the depletion of all components at frequency lower than 2170 cm^{-1} (curves a).

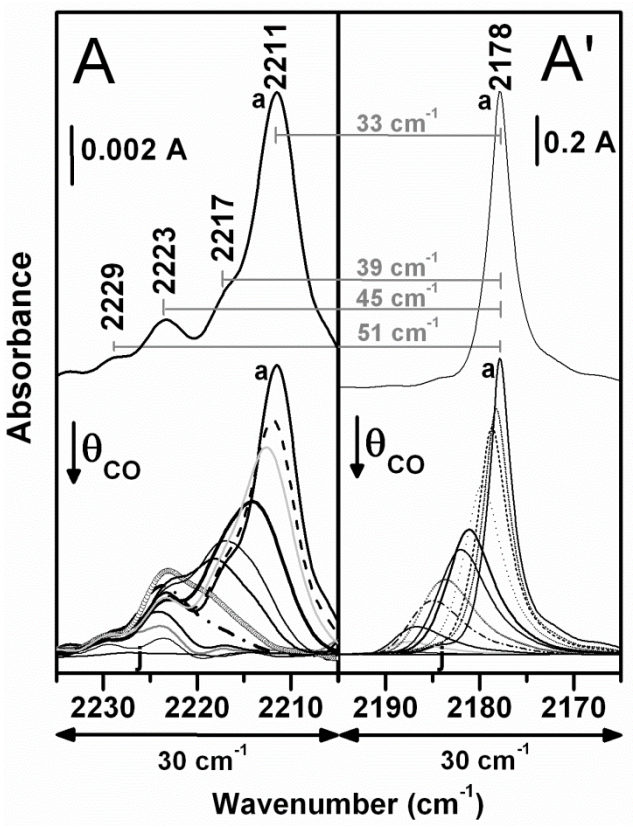

Fig.3 IR spectra, in the 2235-2005 cm^{-1} (panel A), and 2195-2165 cm^{-1} (panel A') ranges, of decreasing amount of CO adsorbed at ca. 100 K on TiO_2 HT outgassed at 873 K. Spectra collected in conditions ranging from the presence of 0.06 mbar (curves a) to outgassing for 10 minutes at ca. 100 K (curves j). Curves **a** have been duplicated and shifted along the Y axis for the sake of clarity (see text).

Focussing on the two ranges of interest, the spectral profile in the 2235-2205 cm^{-1} region (Figure 3A, a) exhibited a main component at 2211 cm^{-1}, with subbands at 2217, 2223 and 2229 cm^{-1}, and no traces of the band due to CO on α sites are present. In the 2195-2165 cm^{-1} range, a definitely narrower band at 2178 cm^{-1}, slightly asymmetric on the lower frequency side, can be observed (Figure 3A', a), without significant contributions from CO on (110) facets. The origin of the 1 cm^{-1} shift with respect to the case of TiO_2 P25 has been previously discussed.[13] By decreasing the amount of adsorbed CO, the peak at 2178 cm^{-1} underwent a progressive up-shift (to ca. 2188 cm^{-1}) and broadening, because of the vanishing of adsorbate-adsorbate interactions, mainly static in origin (Figure 3A', curves a-k).[54] This kind of trend characterized also the evolution of the pattern at higher frequency which, however, appeared more rich and complex (Figure 3A). Likely, the overall behaviour can result from two evolutions, also occurring at the same time: i) the decrease in intensity, broadening and up-shift of components with the consequent overlapping and addition to subbands at higher frequency, and ii) the decrease in intensity of components at lower frequency in favour of the increase in intensity of components at higher frequency. Type (i) evolution seems more likely to occur in the first steps of the removal of CO molecules from the surface of the sample (curves a-d), while type (ii) might prevail in the subsequent steps, and in particular in those corresponding to curves e-g. Moreover, at medium-low CO coverage a shoulder at ca. 2214 cm^{-1} became visible (curve e), then resisting to the further decrease of the amount of adsorbed CO more effectively than the neighbour component at higher frequency at ca. 2217 cm^{-1}. Furthermore, the signals at 2223 and 2229 cm^{-1} exhibited a slight and not monotonous change in position, the latter appearing the less reversible one.

Similar patterns (in terms of number and/or lineshape) and trends in dependence on the CO coverage

were obtained in the case of TiO_2 HT-HF (Figure 4; whole series of spectra of adsorbed CO in Figure S3 in the ESI), indicating that the etching of well-shaped bipyramidal NP of TiO_2 HT resulted in the exposure neither of α sites nor of (110) facets (panels A,A', respectively). Indeed, the similarity between the profile of the νCO band observed for TiO_2 HT and TiO_2 HT-HF (Figures 3A' and 4A', respectively) can appear quite surprising, because of the heavy stepping of (101) facets resulting from the etching (Figure 2C). Nevertheless, it might be considered that formation energy calculations indicated that steps on TiO_2 anatase (101) surfaces exposing only oxygen atoms at the edge should exhibit a higher stability.[12] Hence, stepping of such surfaces does not necessarily imply the formation of new local structures exposing Ti^{4+} with a higher coordinative unsaturation than Ti^{4+}_{5c} at (101) facets.

Conversely, a relevant difference was constituted by the higher relative intensity of the two high frequency components of the 2235-2205 cm^{-1} pattern (panel A), appearing located, at high CO coverage, at 2232 and 2224 cm^{-1} (curve a). Owing to such higher intensity, it was clearly observed that these signals, and in particular the 2232 cm^{-1} one, exhibited a higher resistance when decreasing the amount of adsorbed CO.

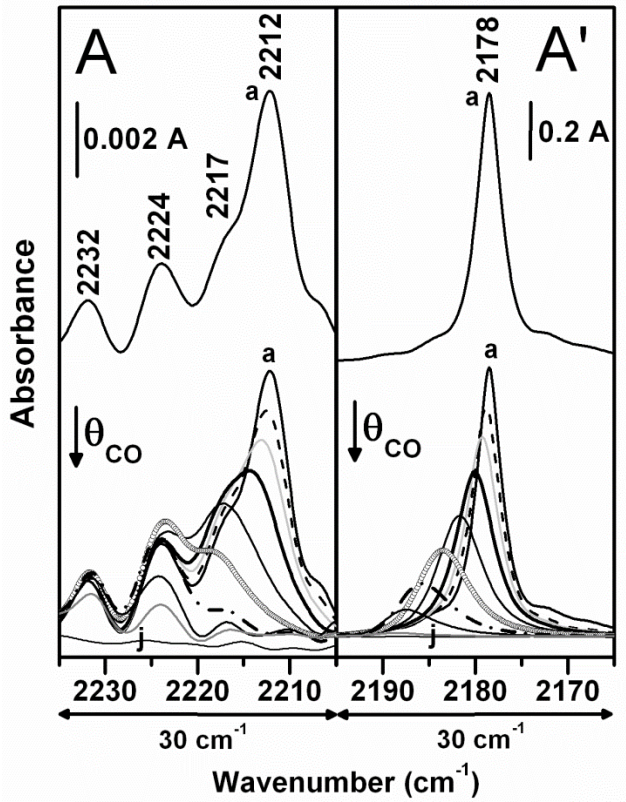

Fig.4 IR spectra, in the 2235-2005 cm^{-1} (panel A), and 2195-2165 cm^{-1} (panel A') ranges, of decreasing amount of CO adsorbed at ca. 100 K on TiO_2 HT-HF outgassed at 873 K. Spectra collected in conditions ranging from the presence of 0.07 mbar (curves a) to outgassing for 10 minutes at ca. 100 K (curves j). Curves **a** have been duplicated and shifted along the Y axis for the sake of clarity (see text).

In summary, the features and behaviour of the very weak pattern in the 2235-2205 cm^{-1} (excluding the part due to CO on α sites present in the case of TiO_2 P25) range described above suggested that it should arise from the combination of internal stretching mode of CO interacting with Ti^{4+}_{5c} exposed at the (101) surfaces - and with Ti^{4+}_{4c} at (110) surfaces in the case of TiO_2 P25 - and one of the low-frequency external modes of adsorbed probe molecules. In order to recognise the actual modes involved in the combination and obtain insights on the origin of the complexity of the resulting spectroscopic pattern, theoretical calculations have been performed.

Theoretical modelling

Calculations on CO/TiO_2 model systems were performed, and, interestingly, vibrational analysis of the normal modes eigenvectors calculated at θ=1 conditions evidenced, on both (101) and (110) surfaces, a huge number of vibrational modes spread over the 900-40 cm^{-1} range. In order to identify the external modes of adsorbed molecules, we need to establish which modes are actually localized on CO. To this aim, an index of mode localization, the Participation Ratio (PR), was calculated for the harmonic modes and reported in Figure 5 for the (101) case. The PR has been calculated first by taking into account the contributions of all the atoms in the system (total PR), and then

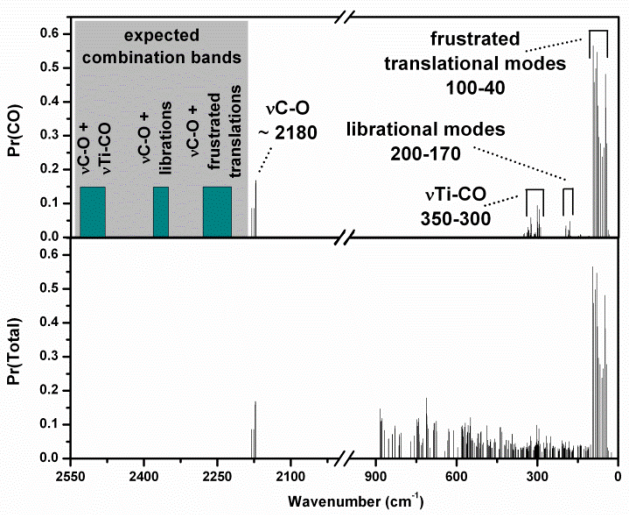

Fig.5 Calculated Participation Ratio (PR) for a θ =1 coverage of CO on (101) TiO_2 anatase slab. Bottom panel: PR obtained by including all the atoms in the system. Top panel: PR obtained by taking into account just the CO atoms.

by considering only the contributions due to the adsorbed CO molecules (partial PR). Since high PR values indicate strong mode localization, modes localized on CO can be identified by comparing the partial PR (Figure 5, top) with the total PR (Figure 5, bottom).

Four spectral regions contain bands localized on CO: the CO stretching region (around 2180 cm^{-1}), the 350-300 cm^{-1}, 200-170 cm^{-1} and 100-40 cm^{-1} regions. Similar results were obtained for the (110) slab (Figure S4, ESI). In both cases, the modes showing stronger localization were in the lowest and in the highest wavenumbers regions, that can be associated with the frustrated translational CO modes and the CO stretching mode, respectively. Moreover, eigenmodes analysis indicated that CO librational modes are in the 200-170 cm^{-1} region, while Ti-CO stretching modes are localized around 350-300 cm^{-1}.

On this basis, we assign the experimental IR pattern in the 2235-2210 cm^{-1} range to combination modes between νCO and the doubly degenerate frustrated translation modes of adsorbed CO molecules (T). Such an assignment is in agreement with what proposed for the case of solid CO.[55] It is also to point out that, since the possible presence of bands at frequency higher than 2250 cm^{-1} has been carefully checked, this is the only combination of νCO with low frequency modes producing an appreciable signal in the 2235-2210 cm^{-1} region. The CO frustrated translation modes, hereafter labelled T1 and T2, are illustrated in Figure 6 top and bottom for the (101) and (110) surfaces, respectively.

Our results indicated that the CO frustrated translation modes are not degenerate and the T1 ones were always found at wavenumbers lower than the T2. Moreover, the T1 and T2 modes maintained very similar frequency values along the whole series of CO/TiO_2 model systems (Table 1). Remarkably, in

passing from perfectly ordered to thermally disordered CO/TiO_2 models, which should be considered for band assignment,[13] both the T1 and T2 modes split in multiple signals roughly centred around the corresponding values obtained for the ordered systems.

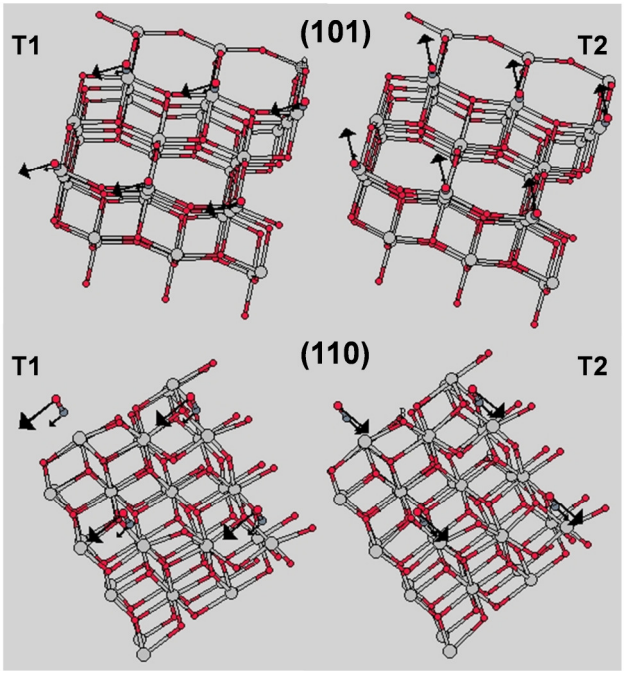

Fig.6 Graphical representation (arrows) of T1 (left) and T2 (right) frustrated translational CO modes on (101) (top) and (110) (bottom) facets. Ti atoms are represented as pale grey spheres, O atoms as dark grey spheres, C atoms as grey spheres.

As an effect, the T bands are spread over a 60 cm^{-1} range. Such a disorder-induced splitting has already been observed for νCO bands on a number of TiO_2 surfaces,[13] but the spanned frequency range was significantly shorter (10 cm^{-1}). On the whole, results in Table 1 indicate that T bands are more sensitive than νCO to disorder effects.

Table 1. Calculated frequencies (cm^{-1}) of frustrated translation CO modes T1 and T2.

	T1	*T2*
θ=1		
(101), ordered CO	45.1	76.5
(101), disordered CO	46.2, 46.9, 47.8, 54.1, 59.0, 66.6	72.5, 76.1, 78.8, 83.7, 89.9, 93.5
(110), ordered CO	38.5	64.5
(110), disordered CO	45.7, 47.9, 49.6, 50.5	60.5, 65.8, 68.8, 71.7
θ=1/6, (101)	40.1	71.2
θ=1/4, (110)	40.0	70.7

Discussion

As a preliminary remark, it can be noticed that in all the considered cases the 2235-2205 cm^{-1} pattern (hereafter indicated as the range typical for the experimental νCO+T combination signals) appeared significantly more complex than the νCO peak in the 2190-2170 cm^{-1} region, as well as its evolution in dependence on the CO coverage. Hence, such differences should be related to the features of the frustrated translational modes occurring in the experimentally inaccessible low frequency region. The experimental values of the frequencies of these modes were calculated from the difference of the maxima of the components of the 2235-2205 cm^{-1} pattern and of the νCO band.

Among the three types of TiO_2 NP considered in the first part of the study, TiO_2 HT, which exhibited quite regular (101) facets, appeared the most suitable for a synergic discussion of experimental and theoretical data, these latter obtained for an ideal surface. In this respect, the various components in the experimental 2235-2205 cm^{-1} νCO+T pattern for $\theta_{CO}(101) \rightarrow 1$, which correspond to frustrated translation frequencies from 33 to 51 cm^{-1} (Figure 3), might be the experimental evidence of a part of the multiplicity of frequencies calculated for CO adsorbed in disordered conditions. However, the theoretical T1 and T2 frequencies are spread over a significantly broader range (ca. 60 cm^{-1}) with respect to the experimental one (ca. 25 cm^{-1}). Remarkably, the experimental frequencies and their spread are very close to the values obtained for the T1 alone, thus suggesting that only the νCO+T1 combination modes could be detected. In order to provide a tentative explanation, it can be observed that the intensity of the components of the 2235-2205 cm^{-1} pattern decreases nearly exponentially with increasing frequencies, approaching the detection limit. Hence, the combinations of νCO with T2 modes, as well as with librational and νTi-CO modes, expected at even higher frequency, might produce signals too weak to be detected.

Let us now pass to the $\theta_{CO}(101) \rightarrow 1/6$ case (Table 1), where calculations indicated that only one T1 (and one T2) frequency should be present, and then contribute to the combination mode. In the experimental spectra, a decrease of the complexity of νCO+T1 pattern occurred, but more components were still present (Figure 3, curves f-j). This feature suggested that an additional source of the multiplicity of the νCO-T1 subbands should be taken into account. In particular, it can be considered that modelled (101) surfaces are ideally perfect and with an infinite extension, whereas (101) facets of TiO_2 HT nanoparticles are limited by edges and exhibited some steps (Figure 2B). Indeed, the part at higher frequency of the νCO+T1 pattern exhibited a significant higher relative intensity in the case of CO on TiO_2 HT-HF, characterized by heavily stepped (101) facets (Figures 2C and 4), clearly indicating the sensitivity of the combination pattern to the surface topography. Noticeably, this behaviour appeared highly relevant if compared with the slight broadening occurring to the νCO band passing from TiO_2 HT to TiO_2 HT-HF (curves a in Figures 3 and 4). *This behaviour highlights the higher sensitivity of frustrated translational modes to different degree of stepping within a given surface.* Such sensitivity might result from the fact that frustrated translational motions explore the in-plane surface features, whereas the internal stretching mode probes the surface perpendicularly.

Another interesting feature is the evolution of the components of the combination pattern while decreasing the CO coverage, characterized by a lower reversibility of the signals at higher frequency which, as indicated on above, should be related to presence of the steps on the (101) surface. Once again, it should be noticed that such a desorption trend is not paralleled by the behaviour of the νCO band, only exhibiting an uniform broadening and up-shifting. Indeed, frustrated translational motions are more directly linked to the steepness of the energy surface potential wells.[20] Accordingly, the signals in the combination pattern which appeared more resistant to CO desorption are those corresponding (in the $\theta_{CO} \rightarrow 1$ limit) to the higher frustrated translational frequencies, which, in turn, are related to steeper potential wells.[20]

Still on the evolution of the 2235-2005 cm^{-1} pattern by decreasing the amount of adsorbed CO, it was

observed that the trend appeared more monotonous in the case of TiO_2 P25 (Figure 1A'). Anyway, it must be noticed that also the progressive shift towards higher frequency of the νCO peak in the 2200-2170 cm^{-1} range appeared less evident because of the presence of the shoulder due to probe molecules on (110) facets, more resistant to the CO outgassing. Theoretical calculations indicated that also frustrated translations of CO on (110) surfaces should occur in the 46-72 cm^{-1} region, therefore they can combine with the νCO mode at ca. 2183 cm^{-1} to contribute to the 2235-2205 cm^{-1} pattern, partly shadowing the evolution of the subbands due to the ν+T1 modes of CO on (101) facets. As a confirmation, in the spectra of CO on TiO_2 P25 pre-outgassed at 573 K instead of 873 K, and then with surface sites on (110) surfaces still occupied by hydroxy groups,[56] the νCO shoulder at ca. 2183 cm^{-1} was almost absent, and by decreasing the CO coverage an evolution of the 2235-2205 cm^{-1} pattern quite similar to what observed for CO on TiO_2 HT and TiO_2 HT-HF was detected (Figure S5 in the ESI).

Conclusions

TiO_2 nanomaterials are strategic for cutting-edge areas of science and technology as well as for a plethora of practical applications; nevertheless, the structural origin of their outstanding properties still is a manifold of open questions. A few of them were addressed herein by considering a set of CO/TiO_2 materials characterized by different structural complexity: the simplest one, TiO_2 HT, with regular facets and well-defined morphology, the intermediate one, a heavily stepped system with regular morphology (TiO_2 HT-HF), and TiO_2/P25, the most complex one. Integrated experimental-theoretical analyses not only provided some clear-cut answers on the presence/absence of specific TiO_2 surface features but also unveiled their connection with low-energy modes of adsorbed CO molecules. We identified, for the first time, a multiple pattern in the 2235-2210 cm^{-1} region, corresponding to the combination bands of νCO with frustrated translational CO modes on TiO_2 facets. Since such spectral region may actually contain components due to other kinds of Ti^{4+} sites, including those with strong Lewis acidity, our study indicates that the appearance of high-energy bands in IR spectra of adsorbed CO may not necessarily be associated to the presence of α sites, providing thus novel guidelines for interpreting IR data of complex TiO_2 materials. Even more importantly, our results reveal that the frustrated translational CO mode, in the 30-50 cm^{-1} range, is much more sensitive than νCO in probing the TiO_2 surface topography and, specifically, the presence of (101) steps. Finally, besides uncovering fundamental aspects of molecular interactions at TiO_2 surfaces, our systematic methodological approach to TiO_2 complexity and the gathered insight opens the way to future work on low-energy modes of adsorbed molecular species. Their great potential as a novel, sensitive and powerful analysis tool for TiO_2 nanomaterials surfaces may foster, in perspective, understanding of the structural leitmotivs underlying titania's reactivity and photocatalytic properties.
At a more fundamental level, our investigations lead to a deeper understanding of interactions of CO/TiO_2 systems at finite temperature conditions, which represents a significant advance for the physical chemistry of molecular adsorption on complex surfaces.

Acknowledgments

The research was funded by Regione Piemonte (Misura I.1.3 "Poli di Innovazione" – III Programma, Polo: MESAP – Meccatronica e Sistemi Avanzati di Produzione; project: GREENPLASMA). Cineca (Bologna, Italy) is gratefully acknowledged for computing grant: ISCRA project HP10BH8BRA "COnTi".

Notes

[a] *Department of Chemistry and Interdepartmental Centre of Excellence "Nanostructured Interfaces and Surfaces-NIS", University of Torino, via P. Giuria 7, 10125 Torino, Italy.*
[b] *Department of Science and High Technology, University of Insubria and INSTM, via Lucini 3, 22100 Como, Italy. Fax: +39 0312386630 ; Tel: +39 0312386618; E-mail:fois@fis.unico.it*

† Electronic Supplementary Information (ESI) available: [(Table S1) calculated surface energies. (Table S2) Assignment of the IR signals of CO adsorbed on TiO_2. (Figure S1) TEM images. (Figure S2) IR spectra of CO adsorbed at 100 K on TiO_2 HT. (Figure S3) IR spectra of CO adsorbed at 100 K on TiO_2 HT-HF. (Figure S4) Calculated Participation Ratio (PR) for a θ =1 coverage of CO on (110) TiO_2 anatase slab. (Figure S5) IR spectra of CO adsorbed at 100 K on TiO_2 P25 outgassed at 573 K. See DOI: 10.1039/b000000x/

References

1. M. Bowker, *Green Chem.*, 2011, **13**, 2235-2246.
2. A. Fujishima, X. T. Zhang and D. A. Tryk, *Surf. Sci. Rep.*, 2008, **63**, 515-582.
3. M. Matsuoka, M. Kitano, M. Takeuchi, K. Tsujimaru, M. Anpo and J. M. Thomas, *Catal. Today*, 2007, **122**, 51-61.
4. M. R. Hoffmann, S. T. Martin, W. Y. Choi and D. W. Bahnemann, *Chem. Rev.*, 1995, **95**, 69-96.
5. M. A. Henderson, *Surf. Sci. Rep.*, 2011, **66**, 185-297.
6. A. Hagfeldt and M. Gratzel, *Chem. Rev.*, 1995, **95**, 49-68.
7. L. Kavan, M. Gratzel, S. E. Gilbert, C. Klemenz and H. J. Scheel, *J. Am. Chem. Soc.*, 1996, **118**, 6716-6723.
8. M. D'Arienzo, J. Carbajo, A. Bahamonde, M. Crippa, S. Polizzi, R. Scotti, L. Wahba and F. Morazzoni, *J. Am. Chem. Soc.*, 2011, **133**, 17652-17661, and references therein.
9. C. H. Chen, R.; Mai, K.; Ren, Z.; Wang, H.; Qian, G.; Wang, Z., *Cryst. Growth Des.*, 2011, **11**, 5221–5226, and references therein.
10. U. Diebold, N. Ruzycki, G. S. Herman and A. Selloni, *Catal. Today*, 2003, **85**, 93-100.
11. V. Shklover, M. K. Nazeeruddin, S. M. Zakeeruddin, C. Barbe, A. Kay, T. Haibach, W. Steurer, R. Hermann, H. U. Nissen and M. Gratzel, *Chem. Mater.*, 1997, **9**, 430-439.
12. X. Q. Gong, A. Selloni, M. Batzill and U. Diebold, *Nat. Mater.*, 2006, **5**, 665-670.
13. C. Deiana, M. Minella, G. Tabacchi, V. Maurino, E. Fois and G. Martra, *Phys. Chem. Chem. Phys.*, 2013, **15**, 307-315
14. R. P. Eischens, S. A. Francis and W. A. Pliskin, *J. Phys. Chem.*, 1956, **60**, 194-201.
15. H. J. Freund, *Faraday Discuss.*, 1999, **114**, 1-31.
16. K. I. Hadjiivanov and G. N. Vayssilov, *Adv. Catal.*, 2002, **47**, 307-511.
17. F. Vindigni, M. Manzoli, A. Chiorino and F. Boccuzzi, *Gold Bull.*, 2009, **42**, 106-112.
18. L. Marchese, S. Bordiga, S. Coluccia, G. Martra and A. Zecchina, *J. Chem. Soc. Faraday T.*, 1993, **89**, 3483-3489.
19. B. N. J. Persson and R. Ryberg, *Phys. Rev. B*, 1985, **32**, 3586–3596.
20. E. Schweizer, B. N. J. Persson, M. Tushaus, D. Hoge and A. M. Bradshaw, *Surf. Sci.*, 1989, **213**, 49-89.
21. S. Briquez, A. Lakhlifi, S. Picaud and C. Girardet, *Chem. Phys.*, 1995, **194**, 65-80.
22. V. Y. Borovkov and H. G. Karge, *J. Chem. Soc. Faraday T.*, 1995, **91**, 2035-2039.
23. H. Steininger, S. Lehwald and H. Ibach, *Surf. Sci.*, 1982, **123**, 264–282.
24. A. M. Lahee, J. P. Toennies and C. Wöll, *Surf. Sci.*, 1986, **177**, 371-388
25. M. Kunat, B. Meyer, F. Traeger and C. Wöll, *Phys. Chem. Chem. Phys.*, 2006, **8**, 1499-1504.
26. C. J. Hirschmugl, G. P. Williams, F. M. Hoffmann and Y. J. Chabal, *Phys. Rev. Lett.*, 1990, **65**, 480-483.
27. D. Hoge, M. Tüshaus, E. Schweizer and A. M. Bradshaw, *Chem. Phys. Lett.*, 1988, **151**, 230-235
28. D. Scarano, G. Spoto, S. Bordiga, A. Zecchina and C. Lamberti, *Surf. Sci.*, 1992, **276**, 281-298.
29. G. Spoto, E. N. Gribov, G. Ricchiardi, A. Damin, D. Scarano, S. Bordiga, C. Lamberti and A. Zecchina, *Prog. Surf. Sci.*, 2004, **76**, 71-146.

30. C. O. Arean, G. T. Palomino, A. Zecchina, G. Spoto, S. Bordiga and P. Roy, *Phys. Chem. Chem. Phys.*, 1999, **1**, 4139-4140.
31. H. H. Richardson, C. Baumann and G. E. Ewing, *Surf. Sci.*, 1987, **185**, 15-35.
32. Y. B. He, A. Tilocca, O. Dulub, A. Selloni and U. Diebold, *Nat. Mater.*, 2009, **8**, 585-589.
33. J. Ryu and W. Choi, *Environ. Sci. & Technol.*, 2008, **42**, 294-300.
34. T. Taguchi, Y. Saito, K. Sarukawa, T. Ohno and M. Matsumura, *New J. Chem.*, 2003, **27**, 1304-1306.
35. K. Hadjiivanov, J. Lamotte and J. C. Lavalley, *Langmuir*, 1997, **13**, 3374-3381.
36. J. P. Perdew, K. Burke and M. Ernzerhof, *Phys. Rev. Lett.*, 1996, **77**, 3865-3868.
37. N. Troullier and J. L. Martins, *Phys. Rev. B*, 1991, **43**, 1993-2006.
38. S. G. Louie, S. Froyen and M. L. Cohen, *Phys. Rev. B*, 1982, **26**, 1738-1742.
39. E. Fois, A. Gamba and E. Spano, *J. Phys. Chem. B*, 2004, **108**, 154-159.
40. E. Fois, A. Gamba and G. Tabacchi, *Chemphyschem*, 2005, **6**, 1237-1239.
41. E. Fois, A. Gamba and G. Tabacchi, *Chemphyschem*, 2008, **9**, 538-543.
42. A. Gamba, G. Tabacchi and E. Fois, *J. Phys. Chem. A*, 2009, **113**, 15006-15015.
43. E. Spano, G. Tabacchi, A. Gamba and E. Fois, *J. Phys. Chem. B*, 2006, **110**, 21651-21661.
44. G. Tabacchi, E. Gianotti, E. Fois, G. Martra, L. Marchese, S. Coluccia and A. Gamba, *J. Phys. Chem. C*, 2007, **111**, 4946-4955.
45. E. Fois, A. Gamba, G. Tabacchi, S. Coluccia and G. Martra, *J. Phys. Chem. B*, 2003, **107**, 10767-10772.
46. E. Fois, G. Tabacchi, D. Barreca, A. Gasparotto and E. Tondello, *Angew. Chem. Int. Edit.*, 2010, **49**, 1944-1948.
47. C. J. Howard, T. M. Sabine and F. Dickson, *Acta Crystallogr. B*, 1991, **47**, 462-468.
48. R. Car and M. Parrinello, *Phys. Rev. Lett.*, 1985, **55**, 2471-2474.
49. *CPMD code, MPI für Festkörperforschung: Stuttgart, Germany; IBM Zürich Research Laboratory: Zürich, Switzerland, 1990-2012, www.cpmd.org.*
50. R. J. Bell and P. Dean, *Discuss. Faraday Soc.*, 1970, **50**, 55-61.
51. M. C. Xu, Y. K. Gao, E. M. Moreno, M. Kunst, M. Muhler, Y. M. Wang, H. Idriss and C. Wöll, *Phys. Rev. Lett.*, 2011, **106**, 138302.
52. S. Coluccia, A. J. Tench and R. L. Segall, *J. Chem. Soc., Faraday Trans. 1*, 1978, **75**, 1769.
53. *Powder Diffraction File JCPDS 21-1272*.
54. G. Spoto, C. Morterra, L. Marchese, L. Orio and A. Zecchina, *Vacuum*, 1990, **41**, 37-39.
55. G. E. Ewing and G. C. Pimentel, *J. Chem. Phys.*, 1961, **35**, 925-930.
56. C. Arrouvel, M. Digne, M. Breysse, H. Toulhoat and P. Raybaud, *J. Catal.*, 2004, **222**, 152-166.